

HAT Discovery of 76 Bright Periodic Variables Toward the Galactic Bulge

D. M. Nataf¹, K. Z. Stanek¹, G.Á. Bakos²,

nataf@astronomy.ohio-state.edu, kstanek@astronomy.ohio-state.edu,
gbakos@cfa.harvard.edu

ABSTRACT

We report on photometric I-band observations of 147 bright ($8 < I < 13$) periodic variables toward the Galactic bulge including 76 new discoveries. We used one of the HATnet telescopes to obtain 151 exposures spanning 88 nights in 2005 of an $8.4^\circ \times 8.4^\circ$ field of view (FOV) approximately centered on $(l, b) = (1.73, -4.68)$. We observed the galactic bulge in 2005 as part of a microlensing feasibility study (Nataf et al. 2009), and here we discuss the periodic variables we found in our data. Among our discoveries we count 52 new eclipsing binaries and 24 other periodic variables.

Subject headings: photometric — bulge — stars: periodic variables: other

1. Introduction

The Galactic bulge is one of the most studied regions of the sky, with recent surveys focused on a broad array of different observables such as deep optical sources (Udalski 2003), the near IR in the context of globular clusters (Valenti et al. 2007), hard X-rays (Kuulkers et al. 2007), γ -rays (Weidenspointner et al. 2008), and extinction toward the Galactic center from the optical through the mid-IR (Nishiyama et al. 2008, 2009), among others. One of the corollary benefits of our small-aperture microlensing feasibility study (Nataf et al. 2009) was the power of a time-series of exposures in a relatively unexplored part of the observational parameter space. What we have with our time-series is a snapshot of bright sources, with apparent magnitudes ranging from 8 to 13 in I . As the distance modulus to the bulge is approximately 14.5 (Stanek & Garnavich 1998; Nishiyama et al. 2006; Bica et al. 2006; Groenewegen et al. 2008; Vanhollebeke et al. 2009; Majaess et al. 2009; Matsunaga et al. 2009) we will be looking at primarily bright stars: bulge giants and brighter main-sequence stars on sightlines toward the bulge but at intermediary distances. This selection effect for brighter stars is amplified by the high extinction toward the bulge. (Sumi 2004), in his analysis of the OGLE-II bulge data, found an extinction of $A_I = (2 \pm 1.5)$. Our observational window overlaps with parts of OGLE-II but also likely include sightlines of much greater extinction.

¹Department of Astronomy, Ohio State University, 140 W. 18th Ave., Columbus, OH 43210

²NSF Fellow, Harvard-Smithsonian Center for Astrophysics, 60 Garden St., Cambridge, MA 02138

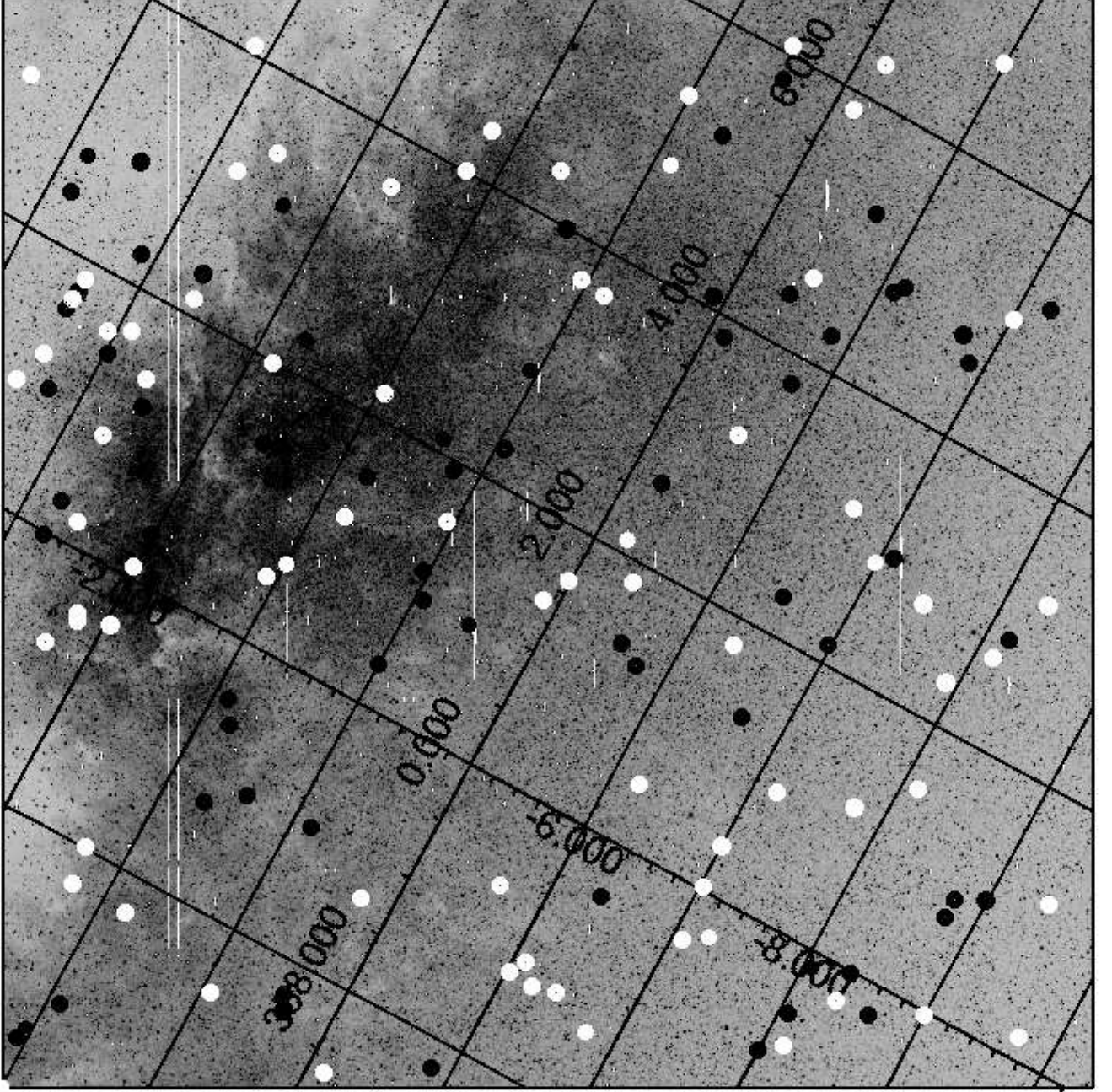


Fig. 1.— Image of our field, with galactic coordinates shown. Of our 147 detected periodic variables, the 71 previously known are shown in black, the 76 new periodic variables are shown in white

Both these populations, the foreground stars toward the bulge and the brightest bulge giants, are independently interesting. With recent findings that the extinction law is a strongly-varying function of galactic position (Udalski 2003; Sumi 2004; Indebetouw et al. 2005; Gao et al. 2009; Zasowski et al. 2009), better understanding of extinction toward the bulge may require anchoring extinction at various points between us and the bulge. Meanwhile, a curious discrepancy has manifested itself between the metallicities of bulge giants and microlensed dwarf stars (Epstein et al. 2010; Cohen et al. 2010) - there may be constraints to be gleaned by having a more complete inventory of the brightest bulge giants.

Our data was taken during the 2005 bulge season, when we obtained 151 exposures. This was done to investigate the idea of Gould & Depoy (1998), that it is feasible for a single wide-field instrument to take high-cadence observations of the brightest stars toward the bulge. That would represent a potential boon for gravitational microlensing, as the highest-magnification microlensing events have an impressive scientific track record of informing exoplanetology, (*e.g.* Gould et al. (2010)). We reproduced several 2005 OGLE-III events toward our field (Udalski et al. 1994), thereby demonstrating the feasibility of a Small Aperture Microlensing Survey (SAMS) and proving the concept of Gould & Depoy (1998), the reader is referred to Nataf et al. (2009) for a more complete analysis. In this paper, we investigate an expected side-benefits of a SAMS, the prospect of acquiring a complete census of the brightest periodic variables toward the bulge. Following extensive reductions, analysis and inspection of our 115,624 point sources, we arrived at a sample of 147 periodic variables. We compared these to the GCVS (Samus et al. 1997), ASAS (Pojmański 2004) catalogs, and OGLE-II variable star catalog (Wozniak et al. 2002) and found that 76 (52%) were previously undiscovered. At least 52 of these are eclipsing binaries. That we obtain such a high yield in the most heavily studied region of the sky with a low cadence and observational span tells us that a large amount of periodic variables remain to be discovered. The yield would have been even higher were it not for overlap with the ASAS variable star search, its southern hemisphere searches between 12th and 18th hour (Pojmanski & Maciejewski 2004) and between 18th and 24th hour (Pojmanski & Maciejewski 2005).

We discuss our data and reduction in section 2, our method of periodic variable selection in section 3, we present our results, discuss some interesting cases and our conclusions in 4. The phased light curves of our new periodic variables along with tables of all observed variables are appended at the end of the paper.

2. Data and Reduction

We closely follow the approach of Hartman et al. (2004). We used the ISIS image subtraction package (Alard & Lupton 1998; Alard 2000) to reduce our data, and the DAOPHOT/ALLSTAR package (Stetson 1992) to construct our source list. Below we list only key points and a generalized overview. A more detailed summary of our data and reduction can be found in Nataf et al. (2009).

Our observations were taken over an 88 day span during the 2005 Bulge season, yielding 151 exposures over 61 distinct nights to image a $8.4^\circ \times 8.4^\circ$ FOV. We used one of the HAT telescopes, HAT-9, located on Mauna Kea, Hawaii. A 11 cm diameter Cannon f/1.8L lens was used to image onto an Apogee AP10 2K \times 2K CCD. The resulting pixel scale is $14''$. A detailed description of the equipment, observing program and preliminary CCD reductions can be found in Bakos et al. (2004). Our photometric precision is shown in Figure 2. Magnitude calibration was done by comparing instrumental magnitudes to photometry of OGLE (Udalski et al. 1997) objects in our field with $I \leq 12.5$. As this is one of the densest fields in the sky blending is a significant concern for the faintest sources, and those with $I > 12$ are more likely to have their brightness overestimated.

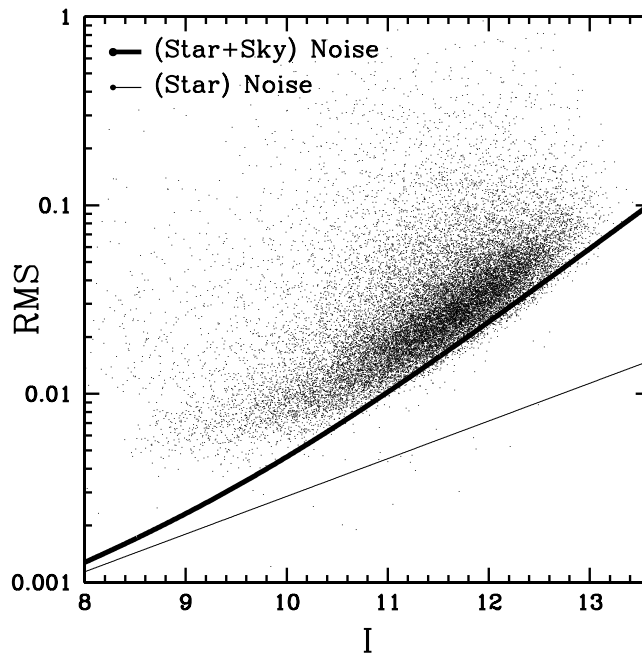


Fig. 2.— The RMS for our light curves is shown as a function of mean magnitude. The theoretical photon-noise limit plotted in the thin black line, and the estimated combined noise from source and sky is plotted in the thick black line.

We performed astrometry on the selected reference frame as described in Pal & Bakos (2006). We sought the astrometric solution in the form of fourth order polynomials connecting the X and Y pixel coordinates with the Cartesian ξ and η (arc-projected) coordinates around the field center, as taken from the 2MASS catalog (Skrutskie et al. 2006). The pixel coordinates of the stars were derived by DAOPHOT. For the brightest sources these pixel coordinates were accurate to ~ 0.03 pixels. The astrometric solution was found by triangle matching, and then refined by matching the $\sim 10,000$ brightest stars on the frame with the 2MASS catalog. The r.m.s. around the best fit is 0.22 pixels (3.2 arcseconds). We then used this astrometric solution to transform all of our (X, Y) coordinates to the World Coordinate System (that of 2MASS, epoch 2000.0, equinox

2000.0), and matched the sources against 2MASS. For stars with a clear match from 2MASS we kept the 2MASS coordinates. For sources with ambiguous or no matches, we keep our projected (X, Y coordinate based) RA and DEC coordinates.

The $(K, J - K)$ color-magnitude diagram for our matches is shown in Figure 2. A few trends are apparent in that figure. First, most of the periodic variables detected, shown as the empty squares (previously known) and the filled circles (new discoveries) are among the bluest stars in CMD, indicating that they are foreground disk stars rather than background bulge stars. Second, the entire CMD spans a broad range in color, $0.0 \lesssim (J - K) \lesssim 2.0$, almost continuously, indicating the high degree of differential reddening. We note that the overdensities in the CMD are not due to red clump stars, but are an artifact of the rapidly declining detection sensitivity to stars fainter than $I = 12$.

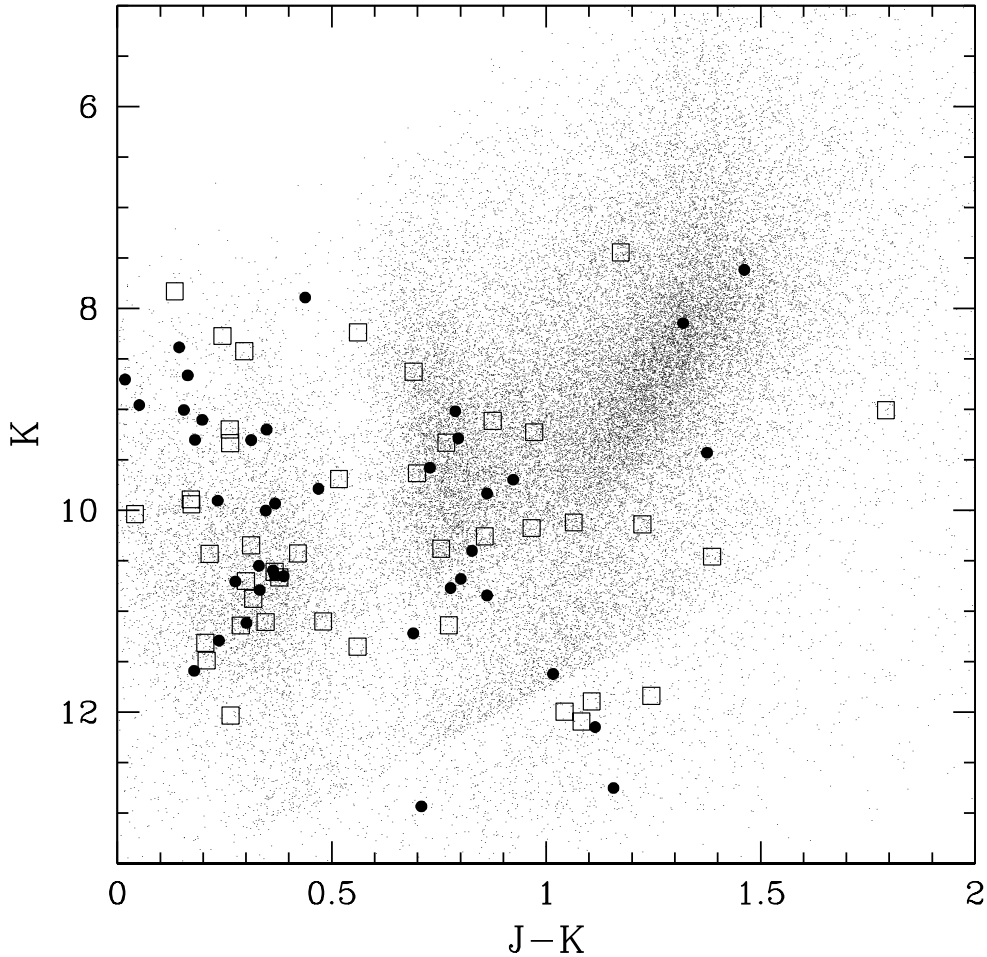


Fig. 3.— 2MASS Color-Magnitude diagram in $(K, J - K)$ for our $\sim 47,000$ matches. The 42 known periodic variables with 2MASS matches are shown as the empty squares, and the 42 new periodic variables with 2MASS matches are shown as the filled circles.

3. Periodic Variable Selection

We ran the Vartools implementation (Hartman et al. 2008) of an analysis of variance (AoV) period search developed by Schwarzenberg-Czerny (1989) and Devor (2005) on our 115,624 sources. We searched for periods between 0.1 and 100 days.

At our sampling - 151 observations spread over 88 nights - aliasing is a significant issue. Many of our lightcurves will exhibit strong Fourier signals for specific periods, particularly at harmonics of 1 day. At the same time, the underlying population of truly periodic variables should have their periods smoothly spread over a periodogram, which should still be the majority of frequency space. Exploiting this, we binned our best-fit periods into 9990 frequency bins covering a range between 0.1 and 100 days. We kept all lightcurves with an empirically-selected variability alarm $\text{AoV} > 3.33$ that had their best-fit period in bins with 25 or fewer lightcurves. That is a generous cutoff, as a uniform distribution would lead to an expectation of only 10 lightcurves per bin. Figure 4 demonstrates the principle.

We discarded 491 of our 9990 bins, 4.9% of frequency space, which in turn contained 80,626 of our 115,624 lightcurves. As such the best variable-extraction performance we could achieve would be $\sim 95\%$ completeness. However, for any realistic cadence, photometric precision and temporal baseline there will be variable classes at the threshold of detection, and these have a higher probability of being shifted into “noise” bins, lowering our expected recovery rate. We manually inspected the 1,588 lightcurves that were in good bins and had an $\text{AoV} > 3.33$, an very low cutoff but rendered possible with the now parsed population of lightcurves. We selected 254 sources, ran a finer AoV search on this smaller sample, and then kept 204 variables.

A systematic issue which crops up in dense fields is that of “variability ghosts”. With blending, a single variable star, if sufficiently bright, may make variables out of multiple nearby stars that are separated by an angular distance smaller or comparable to the width of the PSF. We corrected for this by searching for variable sources within our final list that were nearby to one another, and when the mode of variability was the same we kept the source with the higher amplitude of variation in photon flux.

Figure 4 is a histogram displaying how the remaining lightcurves populated the bins. With $\sim 35,000$ lightcurves and $\sim 9,500$ bins, one would expect an approximately Poisson histogram with a mean of 4, *i.e.* the typical frequency bin would contain the best-fit frequencies to 4 lightcurves. As the remaining distribution is not quite Poissonian one can conclude that even the remaining sample is not “fully cleaned” of bad frequency bins. The Poisson expectation is that virtually no frequency bins contain more than 10 lightcurve matches, whereas we obtain a fair number. Likewise, we also obtain an excess of frequency bins with only 1, 2 or 3 lightcurve matches. We nevertheless chose the cutoff of 25 based on our observations that less generous cutoffs cause the frequency-bin rejection fraction to rise much higher than 5%.

We used the Lomb-Scargle algorithm (Lomb 1976; Scargle 1982; Press & Rybicki 1989; Press et al.

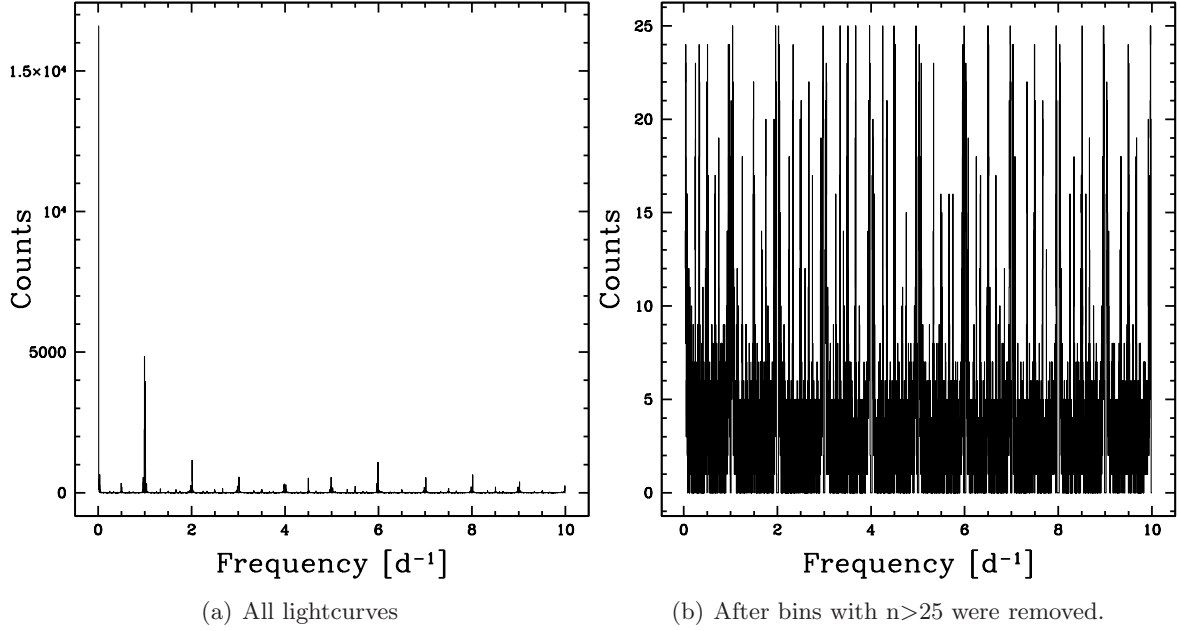


Fig. 4.— Distribution of best-fit frequencies as selected by AoV

1992) as a second means of periodic variable acquisition, in case it could find a few variables missed by AoV. We took the sources which had an $\text{AoV} > 3.33$ but were in congested frequency bins. We first applied a $J_S > 1.2$ cut (Stetson 1996), a measure of correlated variability, thus keeping 11,731 sources. We then ran the Vartools implementation of LS on periods between 0.1 and 44 days, where 11,516 lightcurves (98.2%) were removed for having their best-fit frequency in 49 of the 2000 (5.6%) frequency bins. This left 140 lightcurves which we directly inspected visually. Even then our sample was contaminated. However, it was sufficiently small to be inspected manually. Only 2 of these 140 lightcurve candidates were added to our periodic list, indicating either a high rate of completeness from our AoV search or the fundamental similarity of the two approaches in this observational context.

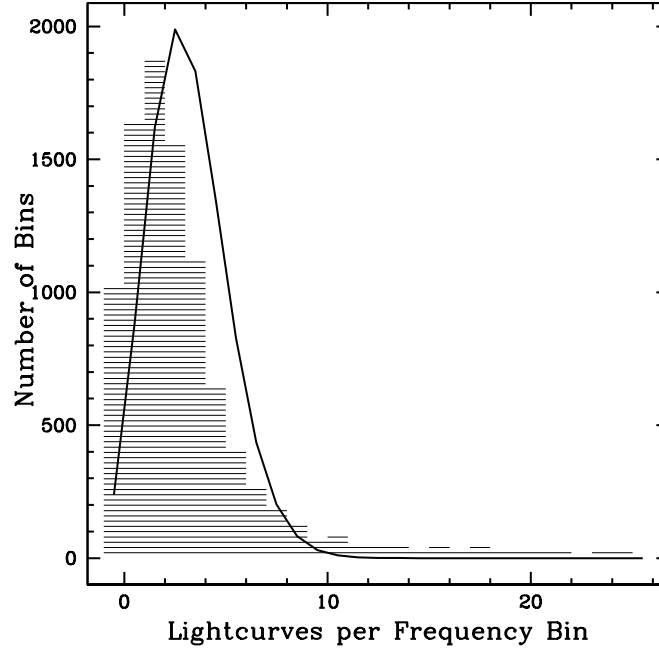


Fig. 5.— Distribution of the lightcurve AoV periods in frequency space. A histogram of the frequencies per bin once bins with $n > 25$ were removed. In red we plot the theoretical expectation based on Poisson statistics.

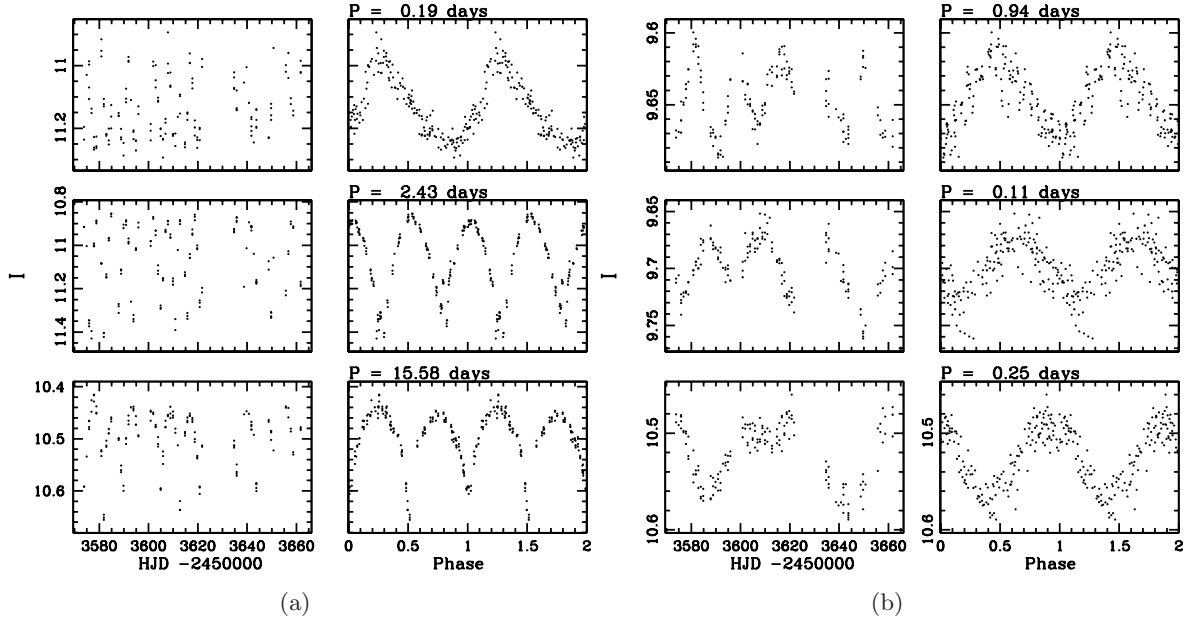


Fig. 6.— On the left, variable stars securely identified as periodic variables. To the right, 3 variable stars well-fit by a likely spurious period due to sampling. The unbinned lightcurves are shown on the left for both sample sets.

The population of bad bins is much more extensive than merely the harmonics of one day. A possible explanation for this is that observations are not really spaced exactly one day apart due to factors such as changing sunset/sunrise time, and the length of the exposure time itself. We had observations on 66 of the 88 nights, with a varying amount of observations per night and of nights between observations. Contamination is thus spread to many other bins, spread densely over the frequency space.

Even after removing bad frequencies, many sources can still be well-fit by a periodic curve in spite of not being true periodic variables, they are likely false positives. We plot 3 cases of such variables in Figure 6(b). It is possible that these sources do possess intrinsic periodicity, perhaps due to rotational brightness modulation, but we could not be sure from our lightcurves alone. Figure 6(b) are a representative sample of more solid finds. Even their unphased lightcurves imply periodicity.

One potential concern is that since the sampling in the time-series generates this issue, perhaps most or nearly all of our periodic variables are spurious? This risk was taken seriously and this is why we opted for a smaller but secure data set rather than a larger but likely contaminated data set. For eclipsing variables, nature has provided an additional means of security - their characteristic shape, which is much less likely to be stochastically mimicked than that of a pulsator. A risk remains some periods could be off by a factor of two, when only one eclipse is visible. In those cases, we chose to assume the binaries were twins, and thus to divide the period into two, rather than that the other possibility, that of a very lopsided surface temperature ratio. Ultimately, a multi-band photometric time series is the best way to resolve this degeneracy.

For our other periodic variables, which are most likely pulsators, we note that we have approximately the same fraction of new discoveries as we do for the more secure eclipsing variables. Some pulsators, such as RR Lyrae, also have characteristic shapes. As seen in Figure 6, lightcurves with more recognizable shapes were also fit with periods further removed from the 1-day frequency harmonics.

4. Discussion & Conclusion

Our find of 76 new periodic variables implies there remains a large number of undiscovered periodic variables toward the galactic bulge, specifically in the brighter magnitude ranges which we explored. As we only had 151 data points, grouped closely together on 66 nights which themselves spanned 88 nights, we expect there to be many more variables which would be extractable with a longer baseline and/or a higher cadence.

In Figure 7 we show the period distribution of our eclipsing binary population and we compare

to that of 10,862 OGLE-II eclipsing binaries cataloged by Devor (2005)¹ for comparison. Our findings are similar with their distribution, which is not obviously expected. The apparent magnitude range of the Devor (2005) sample is approximately $12 < I < 20$, with a median magnitude of ~ 17 - with our range of $8 < I < 13$ we are probing a brighter and thus different population. They are likely probing a different range of stages of stellar evolution, and thus possibly of different initial masses and metallicities, depending on the history of star formation in the bulge. We do note some differences. The mode of our distribution is at ~ 1 day, whereas (Devor 2005) lies at ~ 0.5 days. More observations are needed to ascertain if this is a true property of foreground disk binaries and/or bulge binary giants rather than a statistical fluke. A more complete sample of the bright eclipsing binaries could potentially impose tight constraints on binary evolution models and of the star formation history in the bulge. Using numerical models, Fabrycky & Tremaine (2007) investigated how a binary population period distribution would evolve after 10 billions years from effects such as tidal and 3-body Kozai interactions. They predicted a surge of binaries with periods between 1 and 10 days from 3-body interactions. The larger the fraction of binaries in hierarchical systems with a distant ternary companion, the more significant this effect is expected to be.

We comment on an interesting variable. In Figure 4, we show a known periodic variable, ASAS 182429-3225.6. The ASAS data plotted in green is from one of their 4 cameras, and is in V-band. Both the ASAS plot and our plot exhibit the O’Connell effect, a light asymmetry between successive maxima in an eclipsing binary (O’Connell 1951). It appears more pronounced in I-band. Explaining the O’Connell effect has been one of the challenges in close binary star models, and efforts continue to do so, using models such as captured circumstellar material (Liu & Yang 2003) and starspot activity (Binnendijk 1960; Linnell & Olson 1989; Bell et al. 1990). Some observational and statistical investigation of the effect continues, Pilecki et al. (2007) searched for correlations between the amplitude of the O’Connell effect and period change rates in eclipsing binaries. The poorly understood variation of the amplitude of the O’Connell effect with bandpass may cloud such studies. As the ASAS survey (Pojmański 2004) provides time-series for large-swaths of the bulge in V , and OGLE (Udalski et al. 2008) has its highest cadence in I , a SAMS instrument might maximize its complementary potential by taking data in J or H .

¹Obtained from: <http://www.iop.org/EJ/article/0004-637X/628/1/411/61389.html>

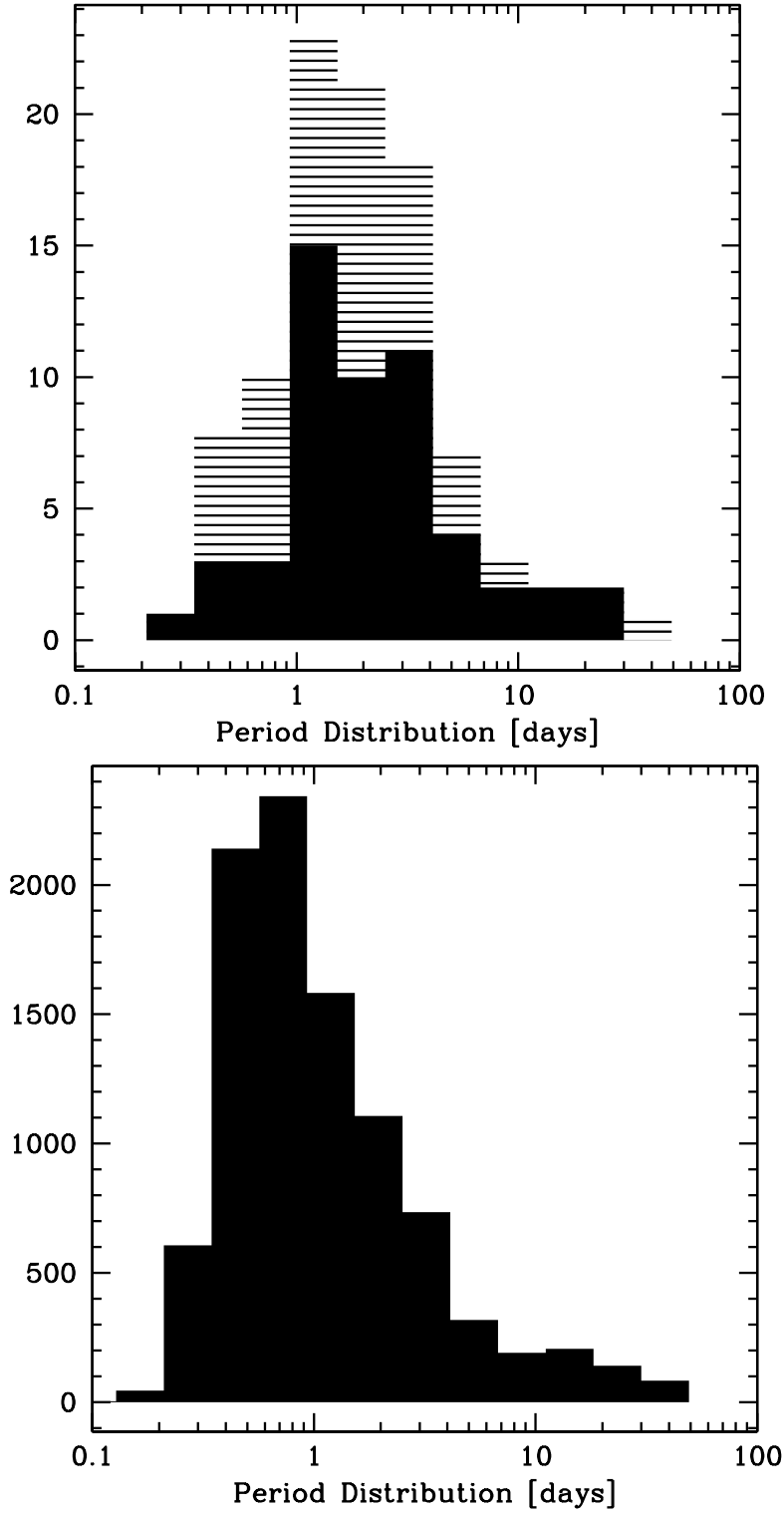


Fig. 7.— Top: The distribution of periods of our final sample of our 52 previously unknown eclipsing variables is shown as the shaded histogram. Adding the eclipsing binaries previously known from ASAS and GCVS yields a sample of 96, seen in the striped histogram. Bottom: We show as comparison the distribution of 9,501 of the 10,862 OGLE-II eclipsing binaries (Devor 2005) that fall within our period range.

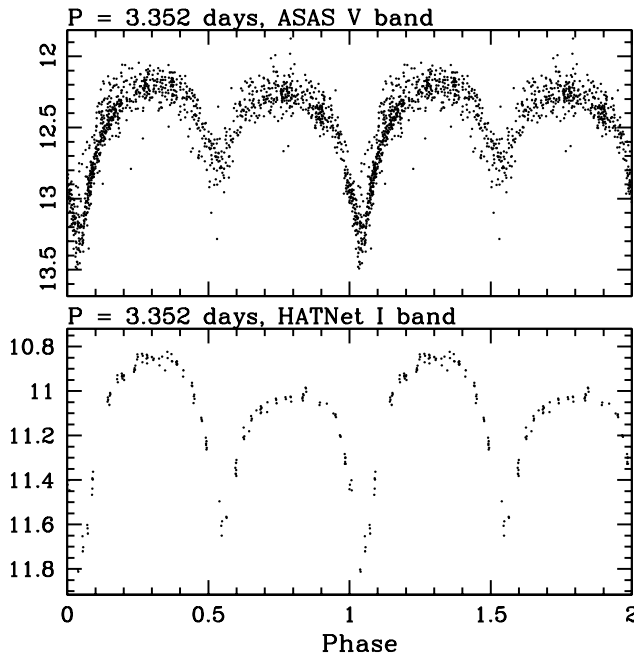


Fig. 8.— An interesting eclipsing binary, HAT-622-37664, located at $(\alpha, \delta) = (18:24:29, -32:25:57)$. On top, we display the ASAS data, observing a different shape to the light curve in the shorter wavelength V-band, where the amplitude of the O’Connell effect is reduced.

Using wide-field I-band observations, a broad PSF and image subtraction we have demonstrated that there remains significant numbers of bright periodic variables of interest not detected in the direction toward the Galactic Bulge. We count 76 discoveries, of which at least 52 are eclipsing binaries, and the rest are likely pulsating variables. Our observational parameters are very similar to what we suggested in (Nataf et al. 2009) as an accompanying survey to current microlensing surveys, which demonstrates such a survey would have the corollary benefit of increasing the number of known periodic variables. As these occupy a specific observational parameter space - higher brightness - they may correlate to a specific region of physical parameter space - giant stars.

DMN is partially supported by the NSF grant AST-0757888.

HATNet operations have been funded by NASA grants NEG04GN74G, NNX08AF23G and SAO IR&D grants. We thank J.D. Hartman for assistance with use of the Vartools package, and G. Pojmanski for his “lc” program. We made use of the Simbad database, operated in Strasbourg, France by the *Centre de Données astronomiques de Strasbourg*.

This publication makes use of data products from the Two Micron All Sky Survey, which is a joint project of the University of Massachusetts and the Infrared Processing and Analysis Center/California Institute of Technology, funded by the National Aeronautics and Space Admin-

istration and the National Science Foundation.

REFERENCES

- Alard, C., & Lupton, R. H. 1998, *ApJ*, 503, 325
- Alard, C. 2000, *A&AS*, 144, 363
- Bakos, G., Noyes, R. W., Kovács, G., Stanek, K. Z., Sasselov, D. D., & Domsa, I. 2004, *PASP*, 116, 266
- Bell, S. A., Rainger, P. P., & Hilditch, R. W. 1990, *MNRAS*, 247, 632
- Bica, E., Bonatto, C., Barbuy, B., & Ortolani, S. 2006, *A&A*, 450, 105
- Binnendijk, L. 1960, *AJ*, 65, 358
- Cohen, J. G., et al. 2010, *ApJ*, 711, L48
- Devor, J. 2005, *ApJ*, 628, 411
- Epstein, C. R., Johnson, J. A., Dong, S., Udalski, A., Gould, A., & Becker, G. 2010, *ApJ*, 709, 447
- Fabrycky, D., & Tremaine, S. 2007, *ApJ*, 669, 1298
- Gao, J., Jiang, B. W., & Li, A. 2009, *ApJ*, 707, 89
- Gould, A., & Depoy, D. L. 1998, *ApJ*, 497, 62
- Gould, A., et al. 2010, *ApJ*, 720, 1073
- Groenewegen, M. A. T., Udalski, A., & Bono, G. 2008, *A&A*, 481, 441
- Hartman, J. D., Bakos, G., Stanek, K. Z., & Noyes, R. W. 2004, *AJ*, 128, 1761
- Hartman, J. M., et al. 2008, *ApJ*, 675, 1468
- Indebetouw, R., et al. 2005, *ApJ*, 619, 931
- Kuulkers, E., et al. 2007, *A&A*, 466, 595
- Linnell, A. P., & Olson, E. C. 1989, *ApJ*, 343, 909
- Liu, Q.-Y., & Yang, Y.-L. 2003, *Chinese Journal of Astronomy and Astrophysics*, 3, 142
- Lomb, N. R. 1976, *Ap&SS*, 39, 447
- Majaess, D. J., Turner, D. G., & Lane, D. J. 2009, *MNRAS*, 398, 263

- Matsunaga, N., Kawadu, T., Nishiyama, S., Nagayama, T., Hatano, H., Tamura, M., Glass, I. S., & Nagata, T. 2009, *MNRAS*, 399, 1709
- Nataf, D. M., Stanek, K. Z., & Bakos, G. A. 2009, *Acta Astronomica*, 59, 255
- Nishiyama, S., et al. 2006, *ApJ*, 647, 1093
- Nishiyama, S., Nagata, T., Tamura, M., Kandori, R., Hatano, H., Sato, S., & Sugitani, K. 2008, *ApJ*, 680, 1174
- Nishiyama, S., Tamura, M., Hatano, H., Kato, D., Tanabé, T., Sugitani, K., & Nagata, T. 2009, *ApJ*, 696, 1407
- O’Connell, D. J. K. 1951, *Publications of the Riverview College Observatory*, 2, 85
- Pál, A., & Bakos, G. Á. 2006, *PASP*, 118, 1474
- Pilecki, B., Fabrycky, D., & Poleski, R. 2007, *MNRAS*, 378, 757
- Pojmański, G. 2004, *Astronomische Nachrichten*, 325, 553
- Pojmanski, G., & Maciejewski, G. 2004, *Acta Astronomica*, 54, 153
- Pojmanski, G., & Maciejewski, G. 2005, *Acta Astronomica*, 55, 97
- Press, W. H., & Rybicki, G. B. 1989, *ApJ*, 338, 277
- Press, W. H., Teukolsky, S. A., Vetterling, W. T., & Flannery, B. P. 1992, *Cambridge: University Press*, —c1992, 2nd ed.,
- Samus, N. N., Durlevich, O. V., & Kazarovets, R. V. 1997, *Baltic Astronomy*, 6, 296
- Scargle, J. D. 1982, *ApJ*, 263, 835
- Schwarzenberg-Czerny, A. 1989, *MNRAS*, 241, 153
- Skrutskie, M. F., et al. 2006, *AJ*, 131, 1163
- Stanek, K. Z., & Garnavich, P. M. 1998, *ApJ*, 503, L131
- Stetson, P. B. 1992, *JRASC*, 86, 71
- Stetson, P. B. 1996, *PASP*, 108, 851
- Sumi, T. 2004, *MNRAS*, 349, 193
- Szymanski, M. K. 2005, *Acta Astronomica*, 55, 43
- Udalski, A., Szymanski, M., Kaluzny, J., Kubiak, M., Mateo, M., Krzeminski, W., & Paczynski, B. 1994, *Acta Astron.*, 44, 227

- Udalski, A., Kubiak, M., & Szymanski, M. 1997, *Acta Astronomica*, 47, 319
- Udalski, A. 2003, *Acta Astronomica*, 53, 291
- Udalski, A. 2003, *ApJ*, 590, 284
- Udalski, A., Szymanski, M. K., Soszynski, I., & Poleski, R. 2008, *Acta Astron.*, 58, 69
- Valenti, E., Ferraro, F. R., & Origlia, L. 2007, *AJ*, 133, 1287
- Vanhollebeke, E., Groenewegen, M. A. T., & Girardi, L. 2009, *A&A*, 498, 95
- Weidenspointner, G., et al. 2008, *Nature*, 451, 159
- Wozniak, P. R., Udalski, A., Szymanski, M., Kubiak, M., Pietrzynski, G., Soszynski, I., & Zebrun, K. 2002, *Acta Astron.*, 52, 129
- Zasowski, G., et al. 2009, *ApJ*, 707, 510

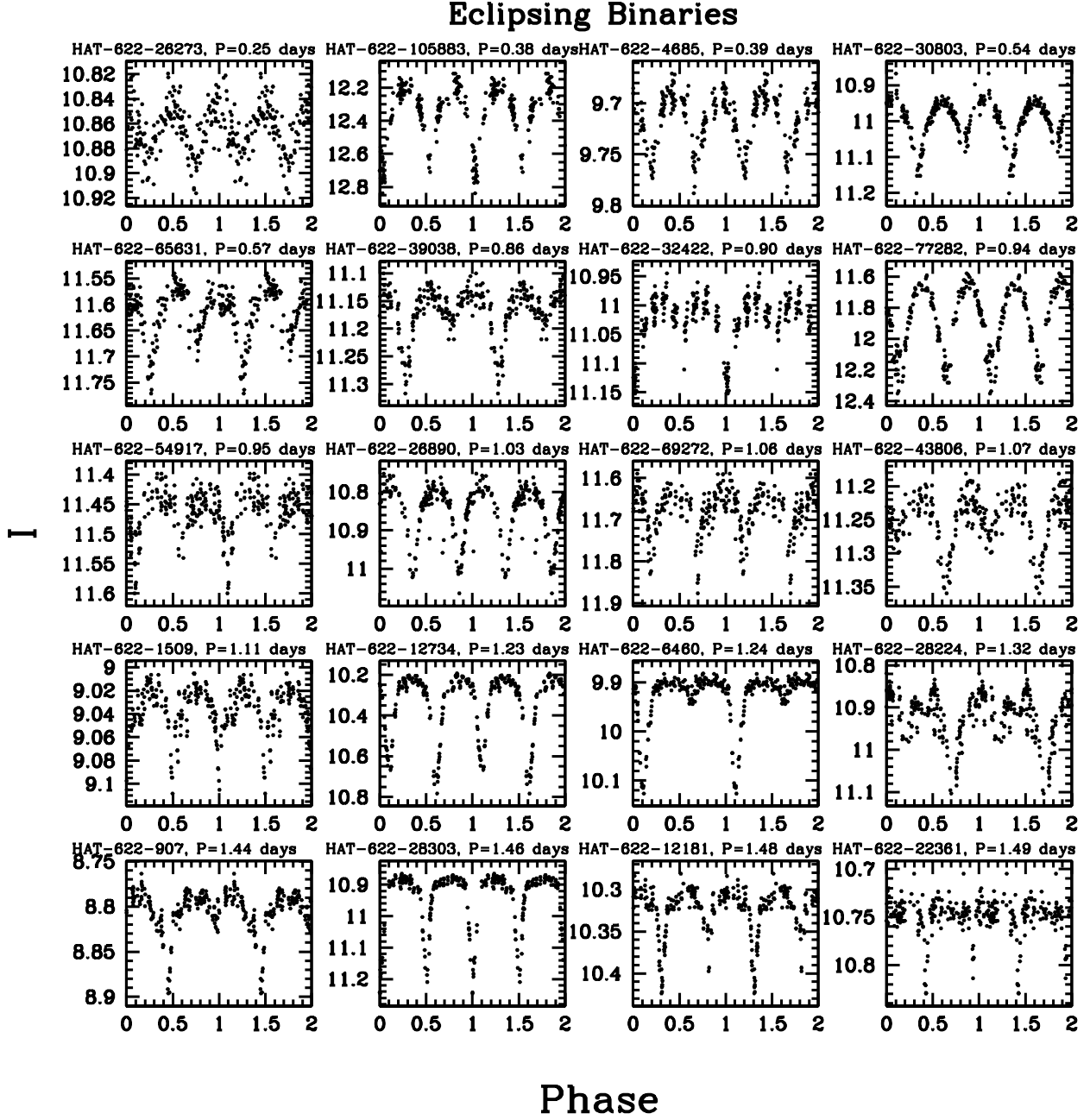


Fig. 9.— Newly discovered eclipsing binaries, sorted by increasing period.

Eclipsing Binaries

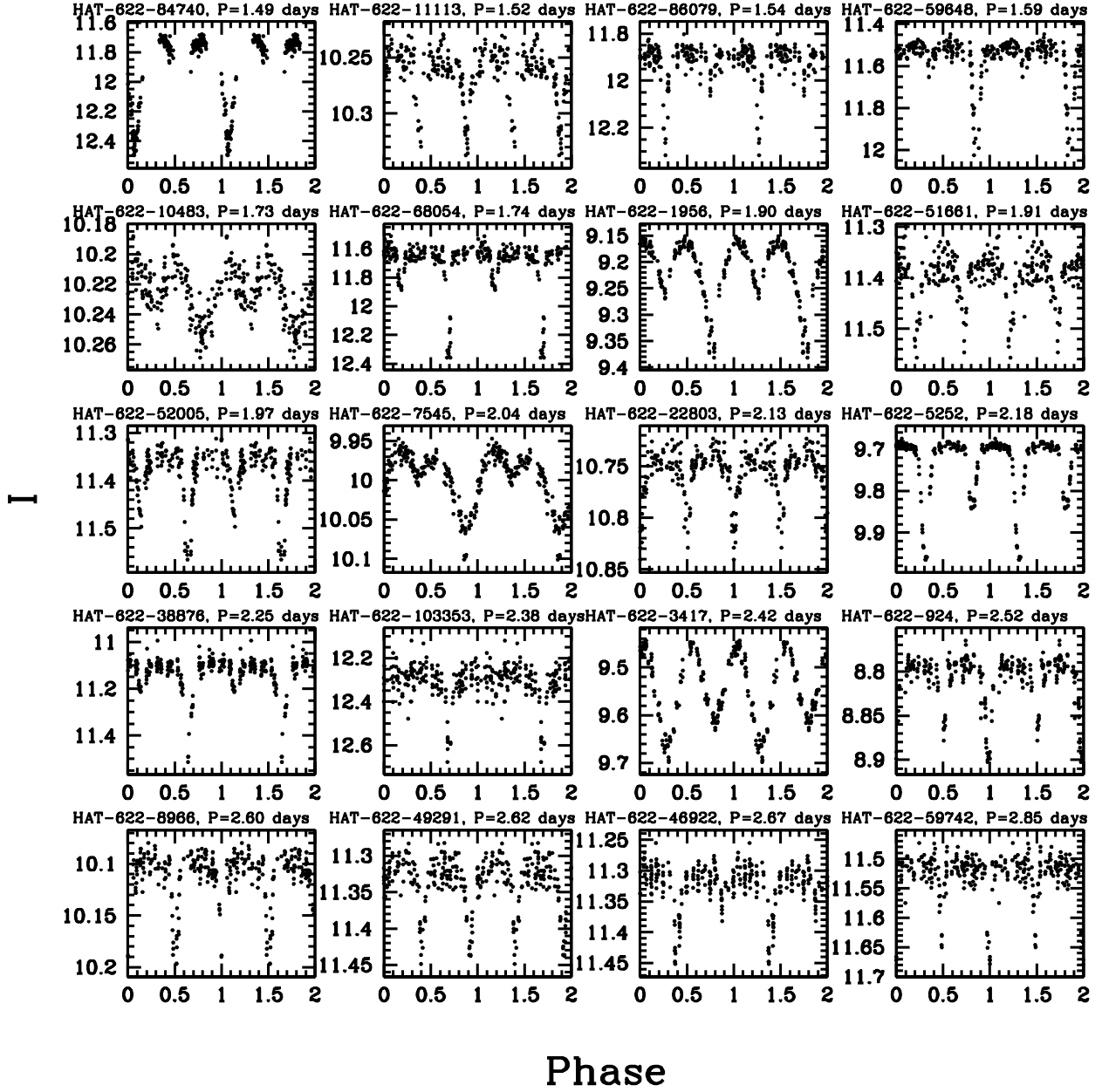


Fig. 10.— Newly discovered eclipsing binaries (continued)

Eclipsing Binaries

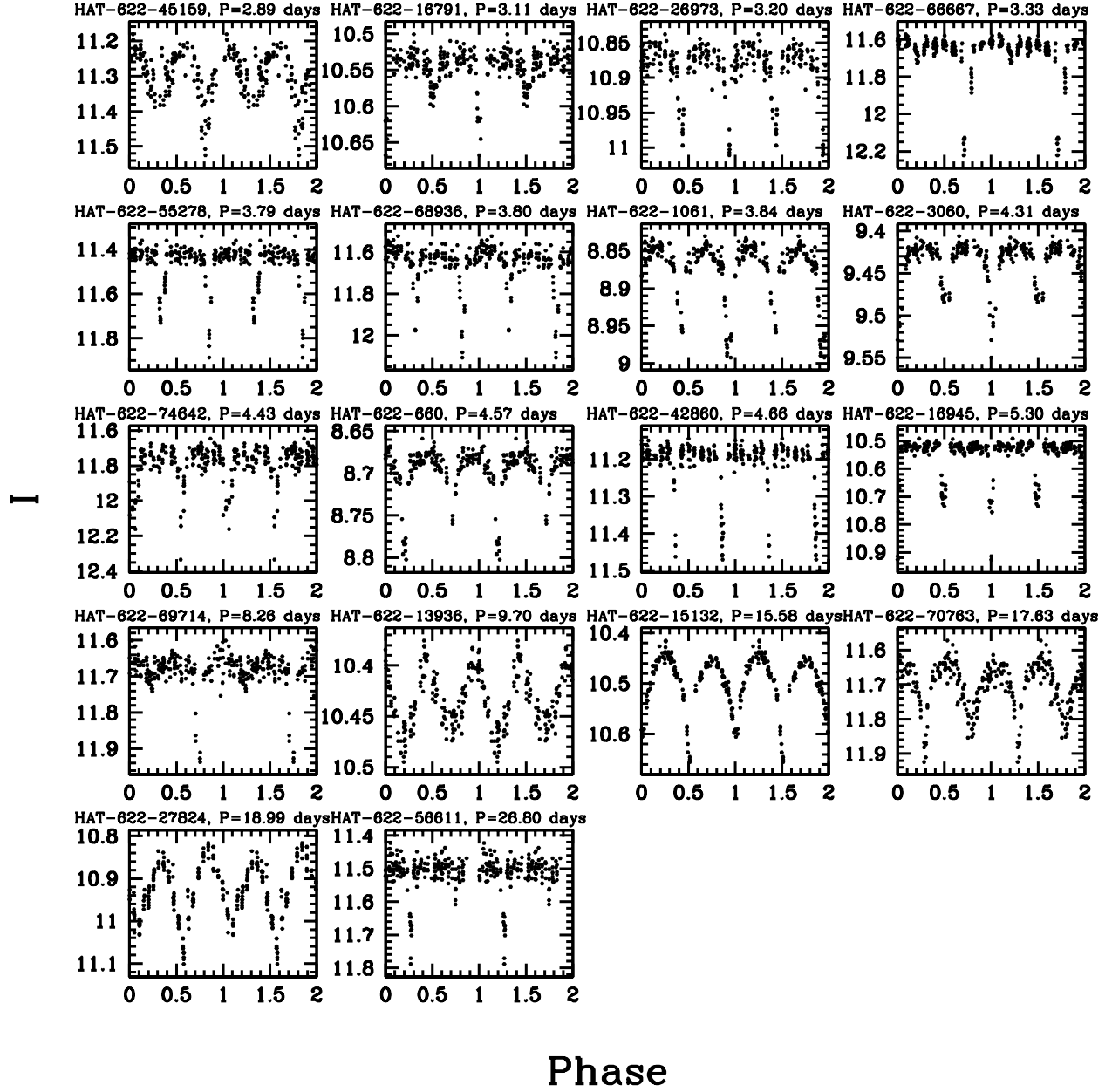


Fig. 11.— Newly discovered eclipsing binaries (continued)

Periodic Variables

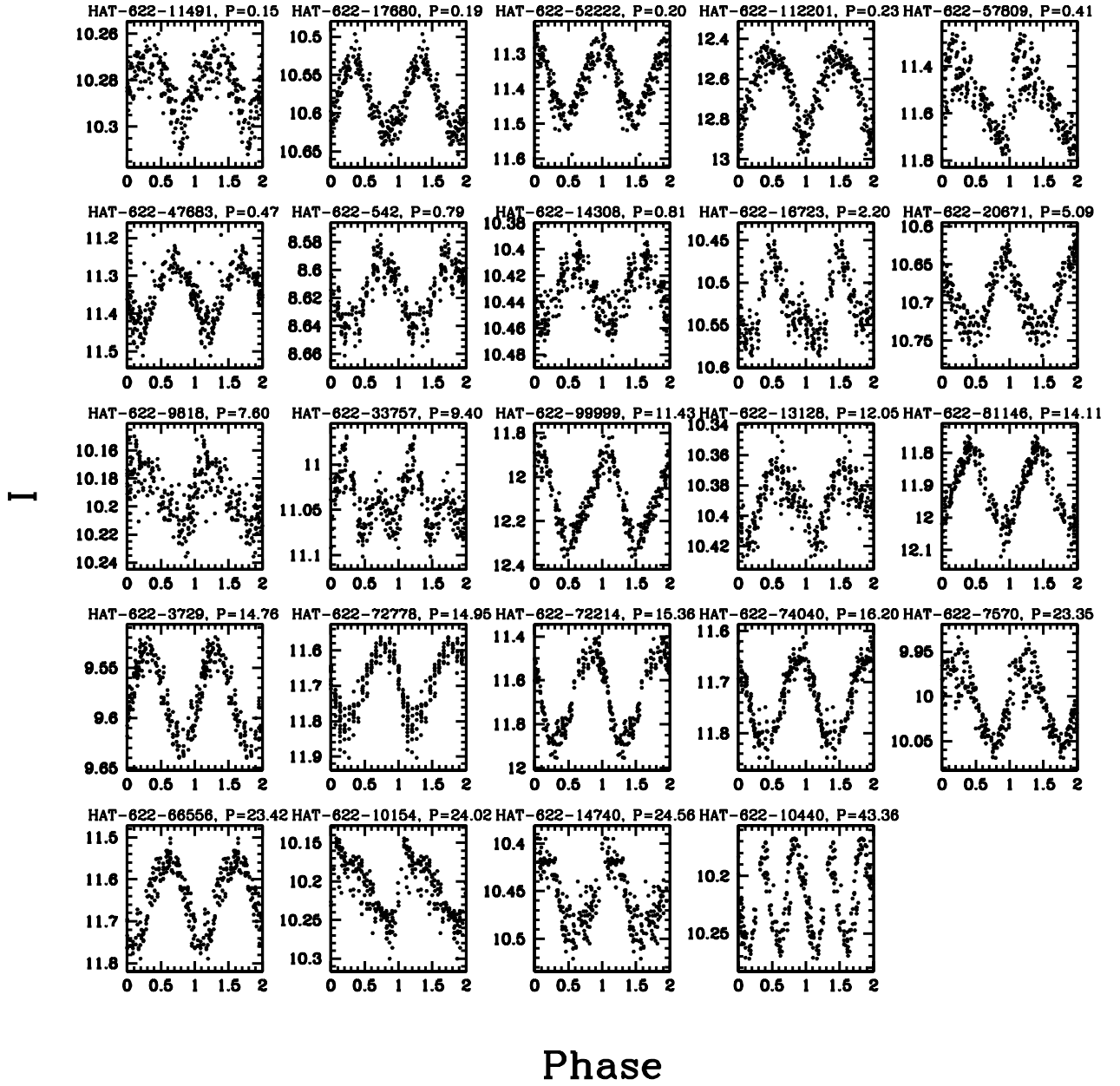


Fig. 12.— Newly discovered periodic variable sources. Additional observations are needed to classify the type of periodicity.

Table 1: Eclipsing Binaries

Name	RA	DEC	I	Period	Status	2MASS ID
HAT-622-159	18:19:36.6	-33:01:19.1	8.268	0.847382	Known	18193663-3301191
HAT-622-660	18:06:42.3	-32:23:03.1	8.69	4.574501	New	18064225-3223030
HAT-622-721	17:58:43.2	-33:19:33.5	8.719	1.788577	Known	17584320-3319335
HAT-622-907	17:51:33.8	-30:17:13.6	8.807	1.43574738	New	17513375-3017135
HAT-622-911	17:58:22.1	-28:57:12.0	8.809	3.385964	Known	17582210-2857119
HAT-622-924	17:51:36.4	-32:02:01.2	8.816	2.516904	New	17513642-3202012
HAT-622-930	17:59:10.4	-27:07:43.2	8.818	0.933608	Known	17591044-2707432
HAT-622-1061	17:49:45.4	-28:24:20.7	8.877	3.836842	New	17494543-2824206
HAT-622-1509	18:08:48.8	-26:51:58.0	9.042	1.112803	New	18084884-2651579
HAT-622-1956	17:54:15.4	-28:26:35.1	9.181	1.89967901	New	17541539-2826351
HAT-622-2503	17:51:51.8	-26:58:53.1	9.322	1.881122	Known	17515178-2658531
HAT-622-3019	18:25:54.7	-27:51:14.5	9.428	1.39468	Known	18255468-2751144
HAT-622-3060	17:52:58.9	-28:03:40.2	9.437	4.309781	New	17525885-2803402
HAT-622-3417	17:51:43.2	-29:31:21.5	9.509	2.42123733	New	17514323-2931215
HAT-622-4685	18:11:44.9	-31:36:12.4	9.706	0.391400	New	18114486-3136123
HAT-622-5252	17:52:59.4	-32:33:10.2	9.779	2.18398710	New	17525940-3233102
HAT-622-6460	18:09:52.1	-33:31:05.6	9.913	1.24266059	New	18095209-3331055
HAT-622-7545	17:53:39.0	-29:53:04.5	10.012	2.03666731	New	–
HAT-622-8870	18:07:44.6	-28:24:04.2	10.115	30.659727	Known	18074457-2824041
HAT-622-8966	18:14:48.1	-32:04:04.9	10.123	2.595499	New	–
HAT-622-9639	18:05:03.0	-29:10:52.7	10.175	1.669197	Known	18050304-2910527
HAT-622-10483	17:56:01.7	-27:50:01.3	10.229	1.72893744	New	17560165-2750013
HAT-622-10793	18:14:33.4	-28:08:46.3	10.249	2.56192	Known	–
HAT-622-11113	18:02:55.9	-26:59:16.0	10.266	1.519982	New	–
HAT-622-11931	18:18:20.0	-28:06:30.6	10.314	6.49587	Known	18181995-2806305
HAT-622-12181	18:24:39.2	-27:56:52.0	10.329	1.47911796	New	–
HAT-622-12734	18:12:38.6	-26:48:52.2	10.359	1.229632	New	18123858-2648521
HAT-622-12906	18:16:27.1	-26:08:44.7	10.368	24.41	Known	18162712-2608446
HAT-622-13936	18:13:13.4	-26:16:23.5	10.421	9.70361754	New	18131340-2616234
HAT-622-14496	18:24:57.4	-30:24:42.6	10.448	2.2517	Known	18245742-3024426
HAT-622-15132	18:19:35.6	-31:44:55.6	10.479	15.5760390	New	–
HAT-622-16791	18:17:12.7	-33:35:29.8	10.549	3.106143	New	–
HAT-622-16945	18:05:33.6	-26:51:43.2	10.555	5.298144	New	18053363-2651432
HAT-622-17137	17:51:09.5	-29:21:19.8	10.563	10.664332	Known	17510954-2921198
HAT-622-20752	18:12:26.4	-29:16:26.7	10.695	1.79772	Known	18122640-2916267
HAT-622-21164	18:11:03.9	-30:30:56.9	10.709	2.45627004	Known	18110385-3030569
HAT-622-21532	17:54:17.5	-29:58:48.4	10.721	2.8617	Known	17541752-2958483
HAT-622-22361	18:19:15.9	-29:26:34.0	10.748	1.487780	New	–
HAT-622-22803	18:15:06.7	-30:30:51.2	10.762	2.130432	New	18150666-3030511
HAT-622-23846	17:59:52.5	-28:09:33.3	10.793	5.100782	Known	–
HAT-622-26273	18:17:39.4	-27:40:11.3	10.863	0.248355	New	18173935-2740113
HAT-622-26342	18:06:51.3	-29:00:12.0	10.865	0.3694	Known	–
HAT-622-26890	18:19:56.9	-26:00:54.8	10.88	1.031726	New	–
HAT-622-26973	18:13:23.9	-32:47:49.8	10.882	3.199622	New	18132385-3247498
HAT-622-27055	17:50:28.9	-33:13:50.0	10.885	1.682458	Known	17502891-3313499
HAT-622-27318	17:49:10.2	-33:24:22.1	10.892	0.79238	Known	–

HAT-622-27824	18:08:16.0	-30:10:37.4	10.907	18.994884	New	18081603-3010374
HAT-622-28224	18:08:46.4	-33:12:37.2	10.917	1.31843018	New	18084639-3312371
HAT-622-28303	18:22:45.3	-30:45:31.3	10.92	1.464364	New	18224531-3045313
HAT-622-29670	17:59:49.6	-31:55:23.8	10.953	1.41833	Known	–
HAT-622-30225	18:16:50.1	-30:08:02.4	10.966	2.42366	Known	18165011-3008023
HAT-622-30286	18:23:00.3	-32:34:03.0	10.968	2.55858224	Known	18230030-3234030
HAT-622-30803	18:20:05.2	-29:51:25.6	10.98	0.54367619	New	–
HAT-622-32374	17:52:00.4	-27:45:08.0	11.016	1.14027	Known	17520035-2745080
HAT-622-32422	18:19:07.3	-33:14:18.3	11.017	0.899283	New	18190730-3314182
HAT-622-37664	18:24:29.2	-32:25:36.5	11.131	3.3517	Known	18242924-3225364
HAT-622-37687	17:50:30.4	-29:36:48.2	11.132	1.433911	Known	17503040-2936482
HAT-622-38876	17:54:20.0	-29:38:15.7	11.156	2.24593272	Known	17541996-2938157
HAT-622-39038	18:21:52.5	-31:35:04.3	11.159	0.86226006	New	–
HAT-622-40871	17:55:57.0	-31:42:45.7	11.196	1.39645	Known	–
HAT-622-41156	17:48:51.0	-33:28:51.6	11.202	0.541165	Known	–
HAT-622-42860	18:10:20.0	-27:49:32.0	11.235	4.657990	New	–
HAT-622-42871	17:56:55.6	-30:55:18.2	11.235	0.395288	Known	17565559-3055181
HAT-622-43806	17:58:19.1	-25:53:33.5	11.254	1.06862778	New	–
HAT-622-45159	17:50:38.8	-26:04:30.3	11.279	2.88845976	New	17503877-2604303
HAT-622-46072	18:02:20.8	-30:40:17.4	11.295	0.569166	Known	–
HAT-622-46260	18:16:56.2	-28:29:29.2	11.298	0.57802	Known	–
HAT-622-46922	18:16:44.0	-31:38:56.1	11.311	2.66821923	New	–
HAT-622-49291	17:59:05.1	-29:53:10.1	11.353	2.615025	New	–
HAT-622-51661	18:00:07.7	-33:48:51.2	11.394	1.905257	New	–
HAT-622-52005	18:21:50.7	-30:09:35.4	11.4	1.974516	New	18215074-3009353
HAT-622-53219	17:58:39.2	-33:20:38.2	11.42	0.421905	Known	–
HAT-622-53272	17:54:46.7	-30:11:24.1	11.421	30.28064	Known	17544667-3011240
HAT-622-54147	18:05:34.3	-30:22:23.9	11.436	1.2335	Known	–
HAT-622-54917	18:16:43.8	-25:53:18.7	11.449	0.954777	New	–
HAT-622-55278	18:14:08.2	-32:22:36.6	11.455	3.786584	New	–
HAT-622-56611	17:52:46.0	-30:19:43.4	11.478	26.801783	New	–
HAT-622-57328	17:52:57.5	-28:13:31.7	11.489	1.15544669	Known	–
HAT-622-59648	17:56:57.9	-31:07:05.7	11.527	1.59332545	Known	17565785-3107057
HAT-622-59742	18:26:17.8	-30:08:19.1	11.529	2.846187	New	–
HAT-622-62542	17:50:48.9	-28:29:23.1	11.575	1.06204	Known	–
HAT-622-65631	18:15:07.1	-28:53:20.6	11.625	0.56969497	New	–
HAT-622-66667	18:23:11.0	-28:17:25.8	11.642	3.32745807	Known	18231095-2817257
HAT-622-68054	18:07:51.2	-33:09:38.4	11.664	1.73587480	New	18075117-3309384
HAT-622-68936	17:52:42.6	-28:51:35.1	11.677	3.796415	New	17524259-2851350
HAT-622-69272	18:18:55.6	-26:21:55.4	11.683	1.064236	New	18185558-2621553
HAT-622-69714	18:26:47.1	-32:25:55.5	11.689	8.25937750	New	–
HAT-622-70763	17:51:49.1	-27:47:59.3	11.705	17.633739	New	–
HAT-622-74308	18:01:59.2	-29:13:38.2	11.764	0.73012	Known	18015915-2913381
HAT-622-74642	17:54:07.1	-28:39:17.2	11.769	4.429529	Known	17540714-2839172
HAT-622-77282	18:08:58.9	-27:19:03.9	11.813	0.942209	Known	–
HAT-622-83009	18:16:16.6	-33:37:48.8	11.907	28.122471	Known	–
HAT-622-84740	17:50:43.2	-28:13:14.3	11.937	1.492609	New	–
HAT-622-86079	17:57:29.9	-31:40:36.9	11.96	1.538337	Known	17572985-3140369
HAT-622-86466	17:51:33.9	-27:52:40.2	11.967	3.209	Known	17513385-2752402
HAT-622-89092	18:11:36.2	-30:41:08.6	12.013	5.52803544	Known	–

HAT-622-91723	18:18:28.8	-30:29:53.7	12.061	1.2989	Known	18182884-3029537
HAT-622-91993	18:20:50.2	-27:43:02.0	12.066	1.472808	Known	18205019-2743019
HAT-622-103353	18:07:39.5	-32:58:45.6	12.31	2.3842397	New	–
HAT-622-104435	18:14:24.4	-26:34:40.8	12.34	0.78628	Known	–
HAT-622-105883	18:09:08.9	-30:02:11.6	12.38	0.384420	New	–

Table 2: Periodic variables of ambiguous classification

Name	RA	DEC	I	Period	Status	2MASS ID
HAT-622-542	17:51:06.8	-32:18:27.7	8.616	0.79162542	New	17510684-3218276
HAT-622-3201	17:54:17.6	-26:45:29.5	9.465	5.7485	Known	17541760-2645294
HAT-622-3729	17:50:24.8	-30:26:24.3	9.564	14.75985462	New	17502475-3026242
HAT-622-7570	17:53:48.1	-28:04:14.6	10.014	23.353579	New	17534805-2804145
HAT-622-9001	18:20:18.4	-33:20:08.4	10.126	5.8241	Known	18201843-3320084
HAT-622-9818	18:04:48.9	-29:34:18.4	10.186	7.59996876	New	18044891-2934183
HAT-622-10154	18:01:11.7	-29:32:02.5	10.208	24.021954	New	–
HAT-622-10359	17:56:21.5	-27:37:55.8	10.221	11.60971	Known	17562148-2737557
HAT-622-10440	18:24:23.1	-30:33:17.6	10.226	43.357149	New	18242310-3033176
HAT-622-11491	17:58:45.8	-28:20:11.4	10.288	0.15498803	New	–
HAT-622-12341	17:58:54.9	-28:58:35.9	10.338	25.687367	Known	–
HAT-622-13128	18:14:22.4	-32:46:12.1	10.38	12.04894357	New	–
HAT-622-14308	17:52:17.4	-27:39:42.2	10.439	0.80660440	New	17521741-2739422
HAT-622-14740	18:07:02.9	-33:03:12.9	10.46	24.55724684	New	18070294-3303128
HAT-622-15750	18:17:19.3	-33:21:03.5	10.505	14.86922	Known	–
HAT-622-16723	17:51:36.1	-30:14:01.7	10.546	2.19533409	New	–
HAT-622-17680	17:59:01.3	-26:43:00.3	10.584	0.19258022	New	17590134-2643002
HAT-622-20671	18:06:27.6	-26:33:09.7	10.692	5.091530	New	–
HAT-622-22364	17:52:28.4	-26:42:12.5	10.748	0.670304	Known	17522840-2642124
HAT-622-24311	18:03:57.9	-29:56:59.8	10.807	0.0844	Known	18035790-2956597
HAT-622-28020	18:20:46.6	-29:48:49.0	10.912	15.04708965	Known	–
HAT-622-28201	17:54:14.6	-27:28:18.9	10.917	16.67188	Known	17541464-2728189
HAT-622-32968	18:15:24.6	-31:04:10.5	11.03	16.20146	Known	–
HAT-622-33757	18:11:27.7	-30:02:11.9	11.048	9.40194621	New	18112766-3002119
HAT-622-34676	18:03:59.0	-30:11:11.8	11.07	0.49126	Known	–
HAT-622-37905	18:04:08.0	-33:46:54.0	11.137	11.59407	Known	18040802-3346540
HAT-622-37992	18:04:41.1	-28:56:04.9	11.138	0.192918	Known	18044112-2856048
HAT-622-40536	18:16:50.3	-27:47:52.7	11.189	0.44087	Known	18165028-2747526
HAT-622-47683	18:24:00.3	-25:58:54.5	11.324	0.46782932	New	18240025-2558544
HAT-622-52222	18:01:36.5	-32:28:42.3	11.403	0.20325365	New	18013650-3228423
HAT-622-57809	18:11:13.6	-29:42:40.3	11.497	1.23919507	New	–
HAT-622-60112	18:19:46.4	-27:09:28.2	11.535	13.91738	Known	–
HAT-622-65557	18:14:08.5	-27:49:31.4	11.624	21.78503371	Known	–
HAT-622-66556	17:56:01.5	-33:10:46.5	11.64	23.42059316	New	–
HAT-622-72214	18:09:32.7	-27:42:15.5	11.729	15.36038098	New	–
HAT-622-72612	18:10:24.0	-32:28:10.5	11.736	22.47432836	Known	–
HAT-622-72778	18:02:37.2	-28:34:38.3	11.739	14.95494757	New	18023717-2834382
HAT-622-74040	17:58:22.2	-29:58:52.8	11.759	16.19772235	New	17582218-2958528
HAT-622-81146	18:25:53.0	-33:27:43.3	11.877	14.11048761	New	18255302-3327433
HAT-622-82362	18:20:26.6	-27:45:41.7	11.897	0.52061004	Known	–
HAT-622-84951	17:58:44.2	-33:11:54.3	11.941	18.319	Known	–
HAT-622-94433	18:23:19.1	-32:25:34.4	12.113	0.58133582	Known	–
HAT-622-96670	18:18:09.0	-32:59:17.4	12.158	12.13572364	Known	18180901-3259173
HAT-622-99999	17:57:36.1	-26:51:13.8	12.23	11.43233439	New	17573613-2651138
HAT-622-104492	18:22:56.3	-28:04:38.7	12.342	14.97269335	Known	–
HAT-622-112201	18:22:22.0	-33:19:16.2	12.64	0.22875900	New	–

Table 3: Properties of known periodic variables with detailed matches in GCVS or ASAS. Some changes to the GCVS classifications made for brevity: Semi-regular pulsating stars have been listed to SRPS, Classical Cepheids (delta Cep) as (δ Cep), and Cepheid variable stars as Cepheid

HAT ID	ASAS ID	ASAS Class.	ASAS P.	GCVS	GCVS Class.	CCVS P.
HAT-622-159	181936-3301.4	EC/ESD	0.847382	-	-	-
HAT-622-721	175843-3319.5	ED	1.788577	V1721 Sgr	EA	1.7886
HAT-622-911	175822-2857.2	ED	3.385964	-	-	-
HAT-622-930	175910-2707.7	EC/ESD	0.933608	-	-	-
HAT-622-2503	175152-2658.9	ED	1.881122	-	-	-
HAT-622-3019	182555-2751.2	ED	1.39468	-	-	-
HAT-622-3201	175417-2645.4	DECP-FU	5.7485	V773 Sgr	(δ Cep)	5.7501
HAT-622-8870	180745-2824.1	ED	30.659727	-	-	-
HAT-622-9001	182019-3320.1	DCEP-FU	5.8241	-	-	-
HAT-622-9639	180503-2910.9	ED/ESD	1.669197	-	-	-
HAT-622-10359	175621-2738.0	DCEP-FU	11.60971	-	-	-
HAT-622-10793	181434-2808.8	ESD/ED	2.56192	-	-	-
HAT-622-11931	181820-2806.5	ED:	6.49587	-	-	-
HAT-622-12341	-	-	-	V5218 Sgr	SRPS	25.00
HAT-622-12906	181627-2608.8	MISC	12.205	-	-	-
HAT-622-14496	182457-3024.7	ESD/ED	2.2517	V5535 Sgr	EB	2.2517
HAT-622-15750	181719-3321.1	DCEP-FU	14.86922	-	-	-
HAT-622-17137	175110-2921.3	ED	10.664332	-	-	-
HAT-622-20752	181226-2916.4	ED/ESD	1.79772	-	-	-
HAT-622-21164	-	-	-	V1178 Sgr	EA	2.458807
HAT-622-21532	175418-2958.9	ESD	2.8617	-	-	-
HAT-622-22364	175228-2642.2	DCEP-FO	0.670304	V767 Sgr	RR Lyr	0.6702
HAT-622-23846	-	-	-	V789 Sgr	EA	2.55234
HAT-622-24311	180358-2957.1	DSCT	0.0844	V5505 Sgr	delta Sct	0.08493
HAT-622-26342	180650-2900.2	EC/DSCT/ESD	0.3694	-	-	-
HAT-622-27055	175029-3313.8	ED	1.682458	-	-	-
HAT-622-27318	174910-3324.3	ED/ESD	0.79238	-	-	-
HAT-622-28020	-	-	-	V741 Sgr	W Vir	15.156
HAT-622-28201	175414-2728.2	MISC	16.67188	-	-	-
HAT-622-29670	175950-3155.3	ED/ESD	1.41833	V994 Sgr	EA	1.4183
HAT-622-30225	181650-3008.0	EC	2.42366	-	-	-
HAT-622-30286	-	-	-	V2537 Sgr	EA	2.5581
HAT-622-32374	175200-2745.1	ESD/ED	1.14027	-	-	-
HAT-622-32968	181525-3104.2	DCEP-FU	16.20146	-	-	-
HAT-622-34676	180359-3011.1	EC/ESD	0.49126	-	-	-
HAT-622-37664	182429-3225.6	ESD	3.3517	-	-	-
HAT-622-37687	-	-	-	V761 Sgr	EA	1.4334
HAT-622-37905	180408-3347.0	DECP-FU	11.59407	V1008 Sgr	Variable Star	11.5918
HAT-622-37992	180441-2856.2	DSCTr/DSCT	0.192918	-	-	-
HAT-622-40536	181650-2747.9	RRAB	0.44087	V1182 Sgr	RR Lyr	0.4409
HAT-622-40871	175557-3142.8	ED	1.39645	V714 Sco	EA	0.6982
HAT-622-41156	174851-3328.9	ESD/EC	0.541165	-	-	-
HAT-622-42871	175656-3055.3	EC	0.395288	-	-	-
HAT-622-46072	180221-3040.4	EC	0.569166	-	-	-

HAT-622-46260	181656-2829.4	EC	0.57802	-	-	-
HAT-622-53219	175839-3320.6	EC -	0.421906	-	-	-
HAT-622-53272	175447-3011.5	MISC	15.14032	V712 Sco	EA	30.3050
HAT-622-54147	180534-3022.5	ED	1.2335	-	-	-
HAT-622-57328	-	-	-	V1603 Sgr	EA	3.3327
HAT-622-60112	181947-2709.4	DCEP-FU	13.91738	V1185 Sgr	Cepheid	13.9125
HAT-622-62542	175049-2829.6	ESD	1.06204	-	-	-
HAT-622-65557	-	-	-	V1181 Sgr	W Vir	21.315
HAT-622-66667	-	-	-	V1603 Sgr	EA	3.3327
HAT-622-72612	-	-	-	V2505 Sgr	W Vir	22.5569
HAT-622-74308	180159-2913.6	EC	0.73012	-	-	-
HAT-622-74642	-	-	-	V5559 Sgr	EA	4.4361
HAT-622-77282	180859-2719.1	EC	0.942342	-	-	-
HAT-622-82362	-	-	-	VV1288 Sgr	RR Lyr	0.5205
HAT-622-83009	-	-	-	V1834 Sgr	W Vir	14.0036
HAT-622-84951	175843-3311.9	DCEP-FU/EC	18.319	-	-	-
HAT-622-86466	175134-2752.6	ED	3.209	-	-	-
HAT-622-89092	-	-	-	V2507 Sgr	E	5.5095
HAT-622-91723	-	-	-	V1184 Sgr	EA	1.2989
HAT-622-91993	-	-	-	V2529 Sgr	EB	0.7363
HAT-622-94433	-	-	-	V1188 Sgr	RR Lyr	0.5813
HAT-622-96670	-	-	-	V2944 Sgr	Variable Star	12.101
HAT-622-104435	181425-2634.7	EC	0.78628	-	-	-
HAT-622-104492	-	-	-	V1187 Sgr	W Vir	15.115